RSC Advances

PAPER

View Article Online
View Journal | View Issue

Cite this: *RSC Adv.*, 2015, **5**, 48983

Synthesis of g-C_3N_4/Bi_2O_3/TiO_2 composite nanotubes: enhanced activity under visible light irradiation and improved photoelectrochemical activity†

Yi Zhang,*[ab] Jiani Lu,[a] Michael R. Hoffmann,[b] Qiang Wang,[a] Yanqing Cong,[a] Qi Wang[a] and Huan Jin[a]

Received 12th February 2015
Accepted 26th May 2015

DOI: 10.1039/c5ra02750k

www.rsc.org/advances

g-C_3N_4 and Bi_2O_3 were successfully incorporated into TiO_2 nanotubes (TiO_2-NT) to produce a composite nanotube material designated as g-C_3N_4/Bi_2O_3/TiO_2. The photoelectrochemical (PEC) activity under visible light irradiation with respect to bleaching of methylene blue (MB) and degradation of phenol were determined. The UV-vis absorption spectrum of the composite material, g-C_3N_4/Bi_2O_3/TiO_2-NT, was red-shifted toward a narrower band gap energy (E_g). The valence band (VB) of g-C_3N_4/Bi_2O_3/TiO_2-NT was shifted to a more positive potential resulting in an increased driving force for water oxidation. The photocurrent generated by g-C_3N_4/Bi_2O_3/TiO_2-NTs was approximately 15 times higher and the incident photon-to-current efficiency (IPCE at $\lambda = 400$ nm) was higher than that of the naked TiO_2-NTs. This response is attributed to increasing the lifetimes of photo-generated electron–hole pairs. A significantly higher PEC response in terms of the bleaching of MB was observed on g-C_3N_4/Bi_2O_3/TiO_2-NT. The roles of improved charge separation and subsequent higher electron-transfer efficiencies for in g-C_3N_4/Bi_2O_3/TiO_2-NT electrodes were examined.

1. Introduction

Semiconductor photocatalysis has been extensively explored for a variety of environmental control applications[1–3] and for solar energy conversion in terms of photocatalytic water-splitting[4,5] and artificial photosynthesis including CO_2 reduction to hydrocarbon fuels.[6] Photoelectrochemical (PEC) activity under an applied potential bias was applied for splitting water or degradation of environmental pollutants. Since 43% of incoming solar radiation is within the visible region, improving solar conversion efficiency over this region is important.[7] For large-scale applications, sustained and in-depth attention has been paid to TiO_2 because the cost is low, stability is excellent and band edge potential is suitable.[8,9] However, since UV light (4% of the solar spectrum) at $\lambda \leq 385$ nm is required to activate anatase TiO_2, the potential practical applications are limited.[10] The modified TiO_2 has been investigated to improve the photocatalytic activity induced by visible light. For instance, doping TiO_2 with metal ions[11,12] or nonmetal ions[13,14] have been employed. Moreover, some non-oxide photocatalysts (*e.g.*, metal sulfides, (oxy) nitrides and oxysulfides)[15,16] and various metal complexes (*e.g.*, Pt, Au or Ag)[17] are quite active under visible light irradiation. However, rapid electron–hole recombination, reduced stability, and high costs of production of the doped metal oxides prevent their larger-scale practical applications.

Recently, compositing with two or more different substances together on TiO_2 has drawn increasing attention to researchers and been confirmed to be an effective approach. Polypyrrole-decorated Ag–TiO_2 nanofibers,[18] Bi_2O_3/$Bi_4Ti_3O_{12}$/TiO_2 nanobelts,[19] Bi_2O_3/TiO_2/graphene composite systems[20] have shown promise for achieving higher visible light photocatalytic activity. In addition, electrochemistry improving the photocatalysis system also has been developed. N and S co-doped into TiO_2 nanotube array films[21] and B and P co-doped TiO_2 nanotube arrays[22] exhibited excellent PEC properties and photocatalytic activities than undoped TiO_2.

Recently, graphitic carbon nitride (g-C_3N_4) was studied having capable of oxidation of pollutants under visible light irradiation.[23,24] Moreover, g-C_3N_4 has high chemical and thermal stability with narrower band gap energy (E_g) of 2.7 eV (ref. 23) than TiO_2. Other researchers have synthesized TiO_2 modified with g-C_3N_4 by chemical vapor deposition[25] or electrodeposition methods[26] to obtain materials that were photoelectrocatalytically active under visible light illumination. Bi_2O_3 is also being explored as a potentially useful photocatalyst due

[a]*School of Environmental Science and Engineering, Zhejiang Gongshang University, Hangzhou 310018, China. E-mail: zhangyi@zjgsu.edu.cn; Fax: +86-571-28008215; Tel: +86-571-28878218*

[b]*Linde-Robinson Laboratories, California Institute of Technology, Pasadena, CA 91125, USA*

† Electronic supplementary information (ESI) available. See DOI: 10.1039/c5ra02750k

to its lower bandgap energy (2.8 eV) and beneficial electrical properties.[27] Bi_2O_3 has also been combined with TiO_2 for improved visible light activity.[28,29] A multi-material composite incorporating g-C_3N_4 and Bi_2O_3 into titanium dioxide nanotubes was prepared and tested in our paper attempting to improve both the photocatalytic and photoelectrochemical activities under visible light irradiation.

Modification of TiO_2 nanotubes (TiO_2-NT) *via* incorporation of g-C_3N_4 and Bi_2O_3 is expected to improve the overall visible light activity when compared to naked TiO_2. Compared to the VB edge of TiO_2 (2.7 V *vs.* NHE (pH = 7)),[30] the band edge of g-C_3N_4 is more negative (1.4 V *vs.* NHE (pH = 7)),[30] while the band edge of Bi_2O_3 is more positive (3.13 V *vs.* NHE (pH = 7)).[31] This combination should improve overall electron–hole separation and improve electron transfer characteristics.

In order to prepare the composite catalyst, we employed a thermal poly-condensation and dip-coating method to modify TiO_2-NTs with g-C_3N_4 and Bi_2O_3. The degradation of methylene blue (MB) and phenol by PEC performance was investigated using a composite catalyst as anode. The PEC performances of the composite electrodes were examined and the photocatalytic (PC) and electrocatalytic (EC) activities under identical reaction conditions were also compared. A mechanism to account for enhanced PEC activity was finally proposed.

2. Experimental methods

2.1. Chemical reagents

Oxalic acid dehydrate ($(COOH)_2 \cdot 2H_2O$) (≥99.5% purity), ammonium fluoride (NH_4F) (≥96.0% purity), melamine ($C_3H_6N_6$) (≥98.5% purity), bismuth nitrate pentahydrate ($Bi(NO_3)_3 \cdot 5H_2O$) (≥99.0% purity), methyl alcohol (CH_3OH) (≥99.9% purity, HPLC, TEDIA company), ethylene glycol ($C_2H_6O_2$) (≥99.5% purity), sodium sulfate (Na_2SO_4) (≥99.0% purity), sodium sulfite (Na_2SO_3) (≥97.0% purity) were all purchased from Hangzhou Huipu Chemical Reagent Co., Ltd.

2.2. Synthesis of g-C_3N_4/Bi_2O_3/TiO_2 nanotubes

Electrochemical anodization method was used to prepare TiO_2-NTs electrodes. The Ti sheet (0.5 mm thick, 99.5% purity) was washed by ultrasonic irradiation for 15 min. The electrochemical reaction was operated using Ti sheet as anode and Ni sheet as cathode with the voltage of 20 V for 120 min. The electrolyte was a mixed solution of 1/12 M $(COOH)_2 \cdot 2H_2O$ and 0.5 wt% NH_4F.[32,33] Metal-free g-C_3N_4 powders were prepared by calcination of melamine to 520 °C for 4 h.[34]

The g-C_3N_4/Bi_2O_3/TiO_2-NTs composites were prepared by a dip-coating method in which 0.2 g g-C_3N_4 and 0.243 g $Bi(NO_3)_3 \cdot 5H_2O$ were dispersed in 20 mL of ethylene glycol solution; the TiO_2-NTs that were still attached to the Ti sheet were slowly dipped up and down from the above solution for 30 min. The dipped coated sheets were then annealed at 400 °C for 2 h.[33] When g-C_3N_4/TiO_2-NTs or Bi_2O_3/TiO_2-NTs were prepared, the precursor solution was changed to 0.2 g g-C_3N_4 or 0.243 g $Bi(NO_3)_3 \cdot 5H_2O$ in 20 mL of ethylene glycol solution.

2.3. Characterization of the synthesized g-C_3N_4/Bi_2O_3/TiO_2 nanotubes

The synthesized materials (TiO_2-NTs, g-C_3N_4/TiO_2-NTs, Bi_2O_3/TiO_2-NTs and g-C_3N_4/Bi_2O_3/TiO_2-NTs) were characterized by X-ray diffractometer (XRD), X-ray photoelectron spectroscope (XPS), emission scanning electron microscope (FE-SEM, Hitachi S-4700 II) with an energy-dispersive X-ray spectrometer (EDX), transmission electron microscope (TEM) and UV-vis diffuse reflectance spectra (DRS).

2.4. PEC experimental techniques

The PEC properties of each sample were determined using an electrochemical workstation (CHI 660D). Modified TiO_2-NTs electrodes were used as working electrodes with saturated Ag/AgCl electrode as a reference electrode and Pt sheet as a counter electrode, respectively. Visible light at an intensity of 100 mW cm^{-2} was obtained by using a Xe-lamp light source with UV filter ($\lambda > 420$ nm). Photocurrents and incident-photon-to-current efficiencies (IPCE) were tested in mixed 0.1 M Na_2SO_4 and Na_2SO_3 solutions at pH of 10.5. IPCE measurements were taken at the visible wavelengths of 400, 430, 450, 475, 500, 550, 600 and 633 nm with a light intensity meter (model FZ-A). Mott–Schottky (M–S) plots and Nyquist plots were taken in 0.1 M Na_2SO_4 solutions at pH = 7.6. M–S plots were obtained at frequencies of 500, 1000 and 3000 Hz at an AC amplitude of 5 mV. Nyquist plots were obtained both under dark and visible light conditions. The experiments including Nyquist plots, LSVs and IPCE plots were repeated for 3 times.

The activity of the prepared catalyst was assessed in three different modes of operation that include (1) photocatalytic (PC), (2) electrocatalytic (EC) and photoelectrocatalytic (PEC). The applied potential in EC and PEC process was 3.0 V. In each case, an electrolyte solution consisting of 0.1 M Na_2SO_4 was irradiated with visible light that had an average light intensity of 200 mW cm^{-2}. MB (100 mL, 1×10^{-5} M, without regulating pH) and phenol (100 mL, 10 mg L^{-1}, pH = 3) fitted with an active electrode with a 4.5 cm^2 effective surface area of g-C_3N_4/Bi_2O_3/TiO_2-NTs. Before initiating the reactions under illumination, the solution reacted with catalyst electrode for 30 min without light. At given time intervals, 3 mL MB and 1 mL phenol aliquot samples were collected. The variation in the MB concentrations was recorded using an UV-vis spectrophotometer. The concentrations of phenol were analyzed by HPLC with a Diamonsil C18 column and ultraviolet detection at 278 nm with ratio of the deionized water and methanol of 6 : 4 (v/v) and a flow rate of 1.0 mL min^{-1}. The overall MB bleaching process and phenol degradation was fitted to pseudo first-order kinetics.

3. Results and discussion

3.1. SEM and TEM analyses

Fig. 1 shows the morphologies of TiO_2-NTs, g-C_3N_4/TiO_2-NTs, Bi_2O_3/TiO_2-NTs, g-C_3N_4/Bi_2O_3/TiO_2-NTs, and pure g-C_3N_4. The TiO_2-NTs electrode has almost uniform holes and a highly ordered tubular structure. The average of the inner diameter of TiO_2-NTs is close to 80 nm, and their average of outer diameter

is near 110 nm. After modification, g-C_3N_4/TiO_2-NTs, Bi_2O_3/TiO_2-NTs, g-C_3N_4/Bi_2O_3/TiO_2-NTs have very similar tubular structures. The g-C_3N_4 powders are likely sheet structures, as shown in Fig. 1(e), accumulating on the surface of g-C_3N_4/TiO_2-NTs. The cross section of the TiO_2 nanotubes was depicted in Fig. 1(f) showing that the mean length of the TiO_2 nanotubes was about 850 nm. Moreover, the EDX analysis (Fig. S1 in ESI†) confirms that Ti, O, C, N, Bi exist in composite material and shows that g-C_3N_4 and Bi_2O_3 are deposited on TiO_2 tubular substrates.

Fig. 2 shows the TEM analysis for g-C_3N_4/Bi_2O_3/TiO_2 composite. The particles also detected in g-C_3N_4/TiO_2 and Bi_2O_3/TiO_2 composites, so g-C_3N_4 and Bi_2O_3 could be found in the nanotubes. And combined with SEM in Fig. 1, the g-C_3N_4 powders also accumulate on the surface of g-C_3N_4/TiO_2-NTs and g-C_3N_4/Bi_2O_3/TiO_2-NTs composites, but little Bi_2O_3 was accumulated on the surface of Bi_2O_3/TiO_2-NTs. It was probably due to that Bi_2O_3 was prepared by anneal of $Bi(NO_3)_3 \cdot 5H_2O$, which may permeate into the tube of TiO_2 and Bi_2O_3 was formed. But g-C_3N_4 was prepared at first and was like the sheet structures, so some small sheets were deposited into the tubes of TiO_2 and some were accumulated on the surfaces of the tubes.

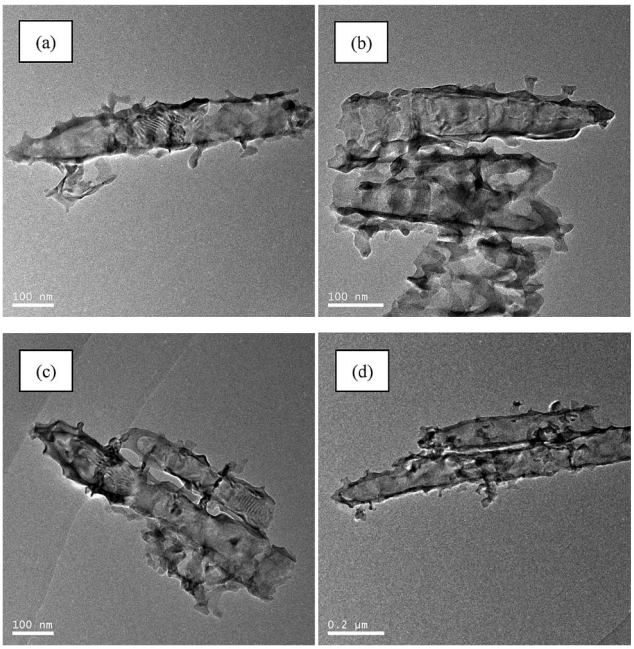

Fig. 2 TEM analysis for g-C_3N_4/TiO_2 (a), Bi_2O_3/TiO_2 (b) and different magnifications of g-C_3N_4/Bi_2O_3/TiO_2 (c and d) composites.

3.2. XRD and XPS analyses

The XRD analysis was applied to detect the formation of TiO_2, g-C_3N_4 and Bi_2O_3 in the composite electrode. However, due to the very low level of incorporated Bi_2O_3, the characteristic peak of Bi_2O_3 in g-C_3N_4/Bi_2O_3/TiO_2-NTs was not seen. In another synthesis the amount of $Bi(NO_3)_3 \cdot 5H_2O$ was increased to 2.910 g in 20 mL of ethylene glycol, which was then dipped coated and annealed to get the fully loaded g-C_3N_4/Bi_2O_3/TiO_2-NTs. Fig. 3 shows the XRD patterns for the TiO_2-NTs and g-C_3N_4/Bi_2O_3/TiO_2-NTs electrodes that were annealed at 400 °C. The peak of $2\theta = 25.2°$ for anatase TiO_2 can be seen in both of the XRD patterns. The characteristic peaks corresponding to g-C_3N_4, Bi_2O_3 are also evident in Fig. 3, which confirms that g-C_3N_4, Bi_2O_3 had been successfully synthesized.

In addition, the XPS analysis of g-C_3N_4/Bi_2O_3/TiO_2-NTs electrode is also depicted in Fig. 4, which showed the existence of Ti 2p, O 1s, C 1s, N 1s and Bi 4f elements. In the inset figure of Fig. 3, two peaks centered at 164.3 and 158.9 eV belong to Bi $4f_{5/2}$ and Bi $4f_{7/2}$ region, which should be determined as Bi_2O_3 species.[35] While, near the main peaks due to Bi^{3+}, there are other two small peaks centered at 157.2 eV and 162.6 eV, which

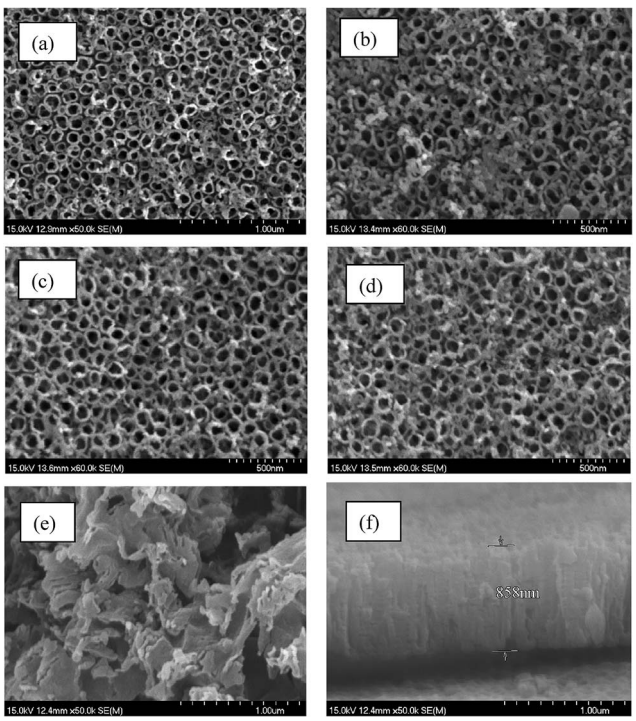

Fig. 1 SEM images of TiO_2-NTs (a), g-C_3N_4/TiO_2-NTs (b), Bi_2O_3/TiO_2-NTs (c), g-C_3N_4/Bi_2O_3/TiO_2-NTs (d), g-C_3N_4 powders (e) and cross section of the TiO_2 nanotubes (f).

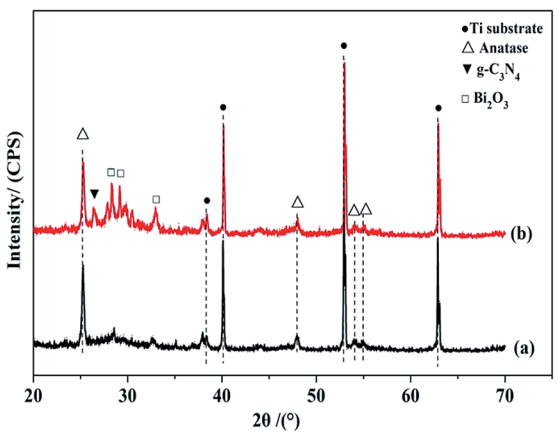

Fig. 3 XRD patterns of TiO_2-NTs (a) and g-C_3N_4/Bi_2O_3/TiO_2-NTs (b).

probably belong to reduced Bi oxidation phase or Bi^0.[36,37] Based on several studies about the reduced Bi phase, it could interact with the structure of Bi oxidation and titania to form the electronic effect between these two oxides.[36,38]

3.3. UV-vis DRS analyses

UV-vis DRS of the composite TiO_2-NTs electrodes modified by g-C_3N_4 and Bi_2O_3 are shown in Fig. 5. The spectrum of g-C_3N_4/TiO_2-NTs is similar to that of unmodified TiO_2-NTs from 220 to 600 nm. While from 220 to 370 nm, the spectrum shows Bi_2O_3/TiO_2-NTs has a lower absorbance when compared to the unmodified TiO_2-NTs, while g-C_3N_4/Bi_2O_3/TiO_2-NTs showed an increase in absorbance compared to naked TiO_2. When wavelength is larger than 370 nm, however, the absorbance of Bi_2O_3/TiO_2-NTs, g-C_3N_4/Bi_2O_3/TiO_2-NTs are higher than that of the naked TiO_2-NTs. In the case of g-C_3N_4/Bi_2O_3/TiO_2-NTs electrode, the absorbance is significantly higher than for the other electrodes in UV-visible region. All of the samples have some degree of visible light absorbance (λ > 400 nm), however this may be due, in part, to the roughness of the electrode surfaces with pores.[39–41]

From Fig. 5, the absorption edges of TiO_2-NTs, g-C_3N_4/TiO_2-NTs, Bi_2O_3/TiO_2-NTs and g-C_3N_4/Bi_2O_3/TiO_2-NTs are located approximately at 382 nm, 388 nm, 400 nm, and 410 nm, indicating that addition of g-C_3N_4 and Bi_2O_3 to the nanotube array extends the absorption to visible range. The corresponding band gap energies were determined using the standard equation as shown belong in eqn (1):[42]

$$\alpha h\nu = A(h\nu - E_g)^{n/2} \quad (1)$$

where α, h, ν, E_g and A are the absorption coefficient, Planck's constant, light frequency, band gap energy, and a constant, respectively. For TiO_2, n is 4 for the indirect transition.[24] Thus, plots of $(\alpha h\nu)^{1/2}$ *versus* photon energy ($h\nu$) are obtained. As shown in Fig. S2,† the E_g of TiO_2-NTs is 3.25 eV, which is similar to anatase TiO_2,[43] while the E_g values for g-C_3N_4/TiO_2-NTs, Bi_2O_3/TiO_2-NTs and g-C_3N_4/Bi_2O_3/TiO_2-NTs are 3.20 eV, 3.10 eV and 3.02 eV, respectively. The UV-vis DRS analysis was detected

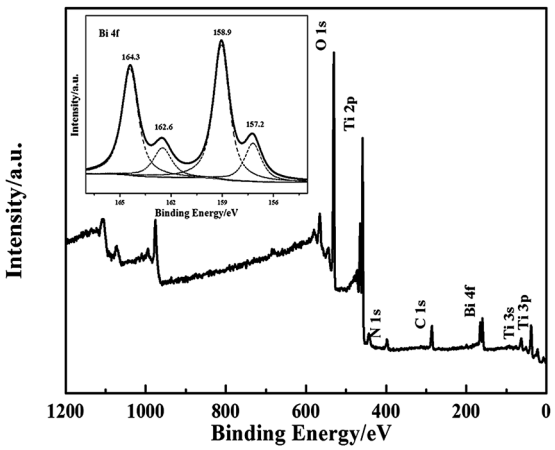

Fig. 4 XPS spectra of g-C_3N_4/Bi_2O_3/TiO_2-NTs.

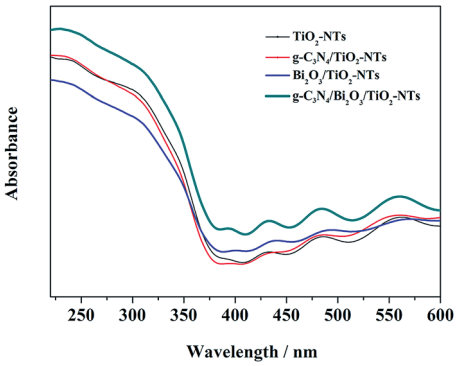

Fig. 5 UV-vis DRS of TiO_2-NTs, g-C_3N_4/TiO_2-NTs, Bi_2O_3/TiO_2-NTs and g-C_3N_4/Bi_2O_3/TiO_2-NTs.

three times and the E_g was changed a little. It was probably that there was a small amount of Bi_2O_3 and C_3N_4 were incorporated with TiO_2 using a dip-coating method, which leads the red shift not significant.[44,45]

3.4. Nyquist and M–S plots

In order to investigate the capacitance and resistance of the electrodes, Nyquist plots of the TiO_2-NTs electrodes as modified by g-C_3N_4 and Bi_2O_3 are shown in Fig. 6. Only one arc was observed for each electrode while the arc radius of g-C_3N_4/Bi_2O_3/TiO_2-NTs was the smallest in dark and visible light irradiation. It implies that interfacial charge transfer is enhanced by a higher efficiency of charge separation.

The M–S plots, as shown in Fig. 7, reveal the flat band potential (E_{fb}) and interfacial charge transfer of the electrode, in which $C_{sc}{}^2$ means the space charge capacitance of the electrode.[46,47] The E_{fb} shifts positively from *ca.* −0.75 V for TiO_2-NTs to −0.40 V for g-C_3N_4/Bi_2O_3/TiO_2-NTs. Similarly, the onset potential of anodic photocurrent shifts positively from *ca.* −0.54 V for TiO_2-NTs to −0.35 V for g-C_3N_4/Bi_2O_3/TiO_2-NTs as shown in Fig. S3.† In both of samples, photocurrent onset potentials are more positive than the E_{fb}. It is probably due to the recombination of electron–hole more quickly for water oxidation, so more positive potentials are achieved for transmission of charge.[48]

The g-C_3N_4/Bi_2O_3/TiO_2-NTs electrode has the highest absorbance and narrowest E_g, as shown in Fig. 5. Combined with E_{fb} and E_g,[32] the VB edge of TiO_2-NTs and g-C_3N_4/Bi_2O_3/TiO_2-NTs electrode is calculated at 2.50 V and 2.62 V, respectively. As a result, the improvement of water oxidation ability of g-C_3N_4/Bi_2O_3/TiO_2-NTs was achieved for the enhancing of PEC properties.[49]

3.5. PEC properties

Linear sweep voltammetry (LSV) method was used to analyze the PEC activities of the composite TiO_2-NTs electrodes. In comparison, LSVs without irradiation were also tested, which shows the surface catalytic property of electrodes for O_2 evolution.[50] From Fig. 8, most of the composite TiO_2-NTs electrodes show a current response until the bias potential is at least 1.0 V

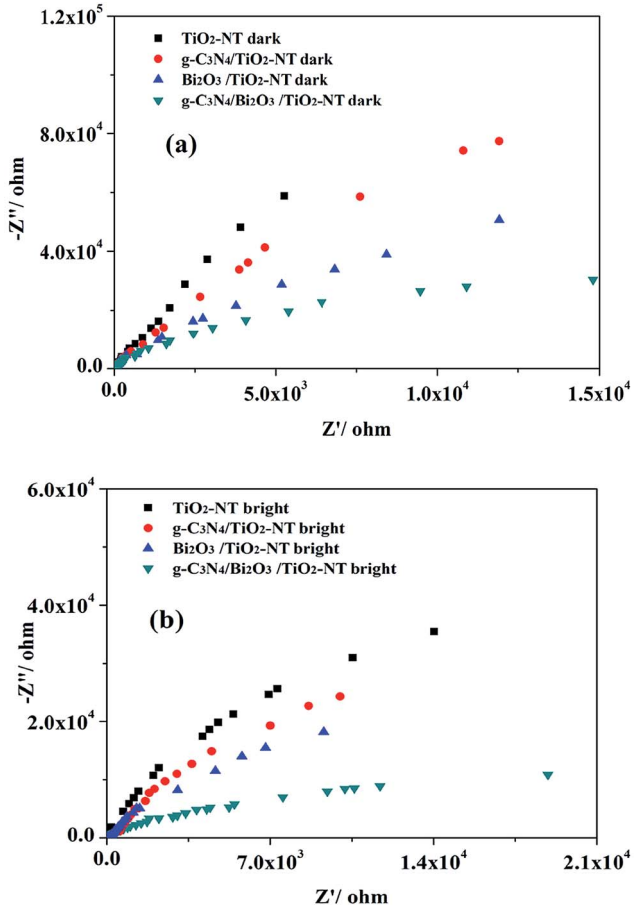

Fig. 6 Nyquist plots of TiO_2-NTs, g-C_3N_4/TiO_2-NTs, Bi_2O_3/TiO_2-NTs and g-C_3N_4/Bi_2O_3/TiO_2-NTsin 0.1 M Na_2SO_4 aqueous solution (pH 7.6) in dark (a) and visible light (b) conditions with a frequency range of 10^{-2} to 10^5 Hz and a scan rate of 5 mV s^{-1}. Light intensity: 100 mW cm^{-2}.

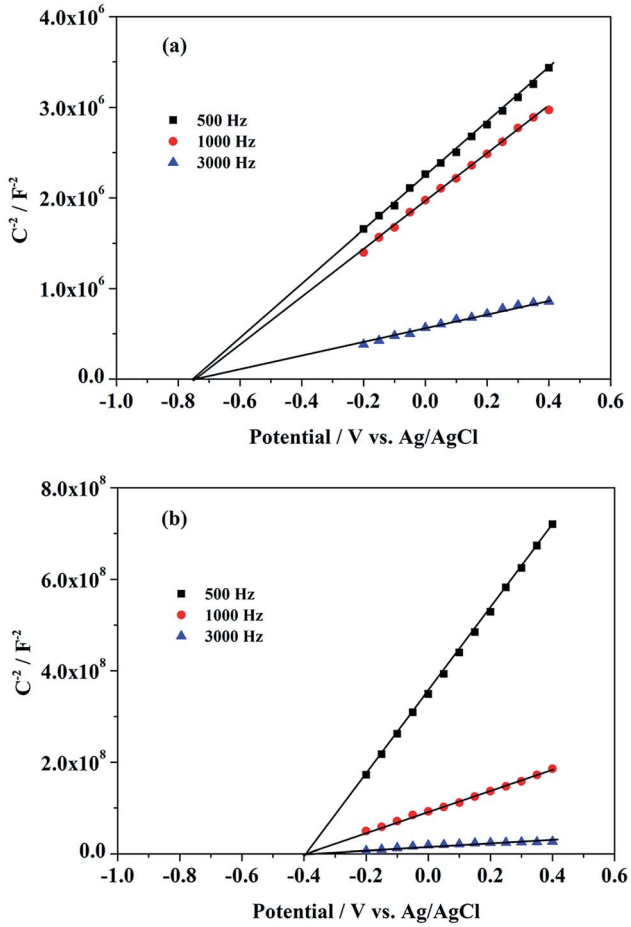

Fig. 7 M–S plots of the TiO_2-NTs (a) and g-C_3N_4/Bi_2O_3/TiO_2-NTs (b) electrodes in 0.1 M Na_2SO_4 aqueous solution (pH 7.6) under dark condition with an AC amplitude of 5 mV at each potential.

without irradiation. The g-C_3N_4/Bi_2O_3/TiO_2-NTs electrode shows a positive shift of the onset potential (Fig. S3†) implying that the surface became easier for O_2 evolution than the unmodified TiO_2-NTs electrodes surface. Moreover, it indicates that the composite electrodes reduced the charge transfer resistance,[50] which is consistent with result of EIS Nyquist analysis in Fig. 6.

Fig. 9 shows LSVs of the composite TiO_2-NTs electrodes under visible light irradiation in 0.1 M Na_2SO_4 and Na_2SO_3 mixture solution. The photocurrent of g-C_3N_4/Bi_2O_3/TiO_2-NTs electrode is *ca.* 15 times larger than that of TiO_2-NTs. Bi_2O_3/TiO_2-NTs electrode has a lightly lower photocurrent compared to g-C_3N_4/Bi_2O_3/TiO_2-NTs, but its photocurrent is still over 8 times larger than that of TiO_2-NTs. The recombination of photogenerated electron–hole decrease with the bias potential increase, and the driving force for photo-generated electrons transferring to the external circuit enhanced. The enhancement of photo-response of g-C_3N_4/Bi_2O_3/TiO_2-NTs electrode under visible light irradiation is probably due to: (1) the higher absorbance and the wider absorption edge; (2) the improved driving force for O_2 production; (3) the improved separation of photo-generated electron–hole pairs.

3.6. IPCE

Fig. 10 shows the IPCE plots as function of wavelength for the composite TiO_2-NTs electrodes calculated by eqn (2):[51,52]

$$\text{IPCE}\ (\%) = 1240 \times (i_{ph}/\lambda P_{in}) \times 100 \qquad (2)$$

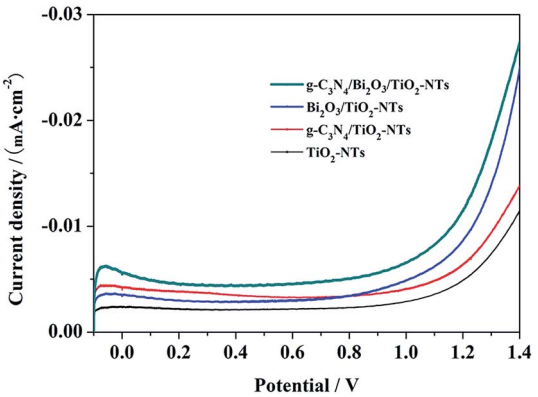

Fig. 8 LSVs of TiO_2-NTs, g-C_3N_4/TiO_2-NTs, Bi_2O_3/TiO_2-NTs and g-C_3N_4/Bi_2O_3/TiO_2-NTs in 0.1 M Na_2SO_4 and Na_2SO_3 mixed aqueous solution (pH 10.5) under dark condition. Scan rate: 10 mV s^{-1}.

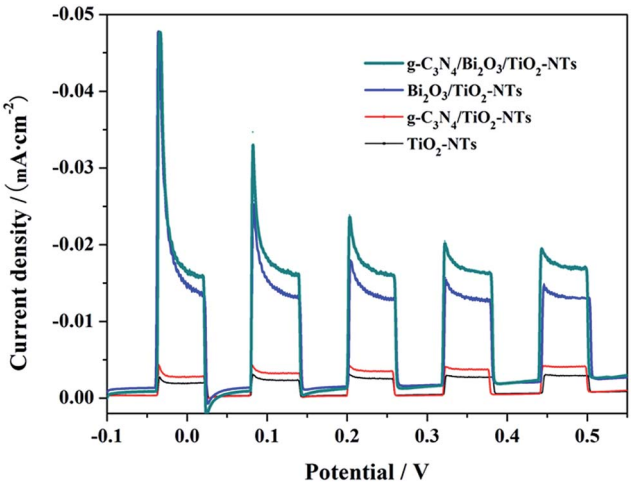

Fig. 9 LSVs of TiO_2-NTs, g-C_3N_4/TiO_2-NTs, Bi_2O_3/TiO_2-NTs and g-C_3N_4/Bi_2O_3/TiO_2-NTs in 0.1 M Na_2SO_4 and Na_2SO_3 mixed aqueous solution (pH 10.5) under chopped visible light ($\lambda > 420$ nm) irradiation. Scan rate: 10 mV s^{-1}. Light intensity: 100 mW cm^{-2}.

where i_{ph} is the photocurrent at 0.40 V (mA), λ is the wavelength (nm) of light, and P_{in} is the light power intensity at λ (mW). The IPCE values decreased with increasing wavelength from 400 to 633 nm. The g-C_3N_4/Bi_2O_3/TiO_2-NTs electrodes show the highest IPCE at 7.59% at 400 nm, which amounts to an enhancement of *ca.* 55% when compared to the unmodified TiO_2-NTs (4.9%).

Zhou's and co-workers[22] have developed boron and phosphor co-doped TiO_2 nanotube arrays (BP-TNTs) by an anodization process on a Ti sheet, achieving the highest IPCE value 3.8% at 400 nm. The same team also prepared a CN/TNT composite heterojunction photocatalyst, which had a maximum IPCE of 7.3% at 400 nm.[26] Jia *et al.*[53] have synthesized polypyrrole (PPy) onto self-organized TiO_2 nanotube arrays (TiO_2-NTs), and the PPy/TiO_2-NTs electrode showed the maximum IPCE of 5% at 410 nm. In contrast, the g-C_3N_4/Bi_2O_3/TiO_2-NTs electrode has higher IPCE in the visible.

3.7. Pollutants degradation

MB and phenol are degraded on the g-C_3N_4/Bi_2O_3/TiO_2-NTs electrode in photolysis, EC, PC and PEC processes, respectively. Fig. 11 shows the removal efficiency of MB at 6.4%, 8.8%, 50.2% and 77.9% after 3 h of reaction in photolysis, EC, PC and PEC process. The corresponding apparent rate constants $k = 0.029$, 0.24 and 0.50 h^{-1} in EC, PC and PEC processes, respectively. The value of k for MB degradation in PEC process is roughly 1.9 times as high as that in (EC + PC) process, indicating that synergistic effect occurred during PEC process. Fig. S4† shows the absorbance spectra of MB degradation at g-C_3N_4/Bi_2O_3/TiO_2-NTs electrode in PEC process. There are three absorption peaks at 292, 246 and 665 nm, in which peak at 665 nm belongs to the auxochrome group of MB and the peaks at 292 nm and 246 nm belong to the substituted benzenes ring structures.[54,55] It can be see that all of the peaks decreased during the reaction, which implied that the MB was bleached and the benzenes ring structures were also decomposed. In addition, before 235 nm, the absorbance spectra of MB increased with time increasing, which possibly shows that some substituted benzene derivatives or other intermediate products may be formed. The analysis of the intermediates needs further investigation.

In addition, the colorless organic phenol also was degraded efficiently in PEC process by using g-C_3N_4/Bi_2O_3/TiO_2-NTs electrode as shown in Fig. S5.† Fig. S6† shows HPLC of phenol degradation at the g-C_3N_4/Bi_2O_3/TiO_2-NTs electrode in PEC process. Compared with the standard compounds, hydroquinone and benzoquinone were produced after degradation as depicted in Fig. S6.† It probably indicated that phenol was degraded to form hydroquinone and then transformed to benzoquinone, and then the benzene rings were opened to form small molecular acids and finally could be mineralized.

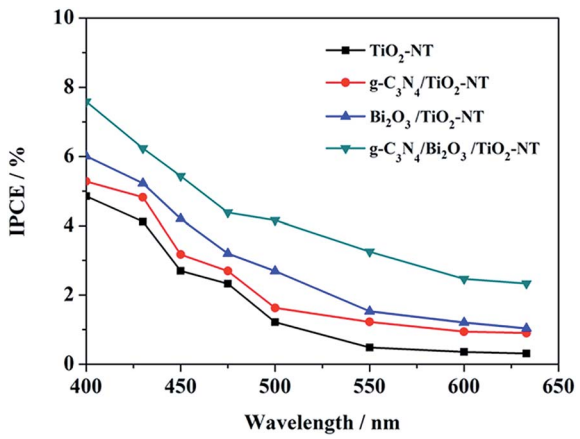

Fig. 10 IPCE plots of TiO_2-NTs, g-C_3N_4/TiO_2-NTs, Bi_2O_3/TiO_2-NTs and g-C_3N_4/Bi_2O_3/TiO_2-NTs calculated from the photocurrent in 0.1 M Na_2SO_4 and Na_2SO_3 mixed aqueous solution (pH 10.5) at an applied potential of 0.40 V *vs.* Ag/AgCl. Light intensity: 100 mW cm^{-2}.

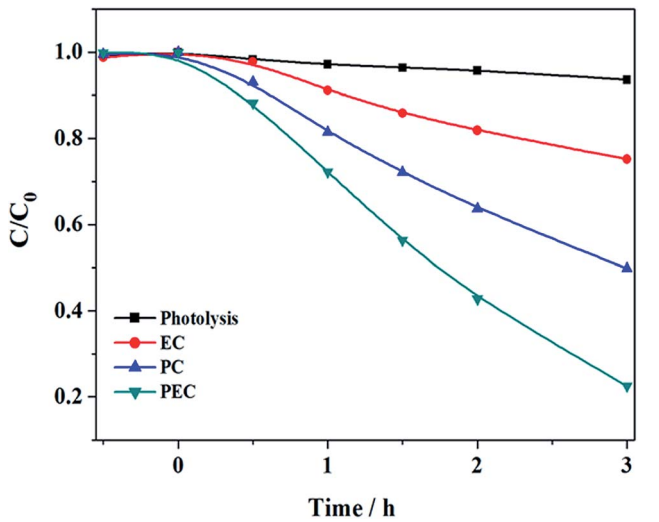

Fig. 11 Variation of [MB] concentration *vs.* time at the g-C_3N_4/Bi_2O_3/TiO_2-NTs electrode in EC, PC and PEC processes. Applied potential: 3.0 V. Electrolyte: 0.1 M Na_2SO_4, pH = 7.6.

Fig. 12 shows the concentration change of MB with different modified TiO_2-NTs electrodes in PEC process. Correspondingly, the removal efficiency of MB is 37.3%, 41.1%, 55.3% and 77.5% for TiO_2-NTs, g-C_3N_4/TiO_2-NTs, Bi_2O_3/TiO_2-NTs, and g-C_3N_4/Bi_2O_3/TiO_2-NTs after 3 h of reaction. Hence, the g-C_3N_4/Bi_2O_3/TiO_2-NTs electrode could contribute to the promotion of the PEC performance compared with TiO_2-NTs electrode.

To check the stability of g-C_3N_4/Bi_2O_3/TiO_2-NTs electrode, MB degradation using the PEC process was repeated for four times. As shown in Fig. 13, the degradation reaction is repeatable through four PEC reaction cycles. This indicates that g-C_3N_4/Bi_2O_3/TiO_2-NTs electrode is reasonably stable during PEC processing.

3.8. Possible considerations

Based on the above results, suggested mechanism for charge separation and electron transfer in g-C_3N_4/Bi_2O_3/TiO_2-NTs electrode is depicted schematically in Fig. 14. The bottoms of the conduction band (CB) of TiO_2, Bi_2O_3 and g-C_3N_4 are located at about −0.5 V, +0.33 V, −1.3 V *vs.* NHE (pH = 7), respectively.[30,31] The E_g of Bi_2O_3 (2.8 eV) and g-C_3N_4 (2.7 eV) are smaller than that for TiO_2 (3.2 eV). Thus, only Bi_2O_3 and g-C_3N_4 can absorb photons and excite photoelectrons under visible light irradiation. One of possible mechanisms is that TiO_2 is placed between Bi_2O_3 and C_3N_4, which has advantage to electron–holes transfer. As shown in Fig. 14(a), with the accumulation of valence holes of Bi_2O_3, the photo-induced holes of Bi_2O_3 flow into the VB of the TiO_2 layer and then into the VB of the g-C_3N_4. Holes on the g-C_3N_4 surface can also degrade MB, giving rise to enhance photocatalytic activity.[56,57] Meanwhile, the electron injection is transferred from the CB of g-C_3N_4 into that of TiO_2 and subsequently could be shuttled freely along g-C_3N_4/Bi_2O_3/TiO_2-NTs matrix of the electrodes to the external circuit, enhancing the separation of electron–hole pairs. Moreover, photo-generated electrons of Bi_2O_3 can react with oxygen molecules to generate superoxide $O_2^{\bullet-}$, which leads to H_2O_2 production and eventual bleaching of MB. Even though the TiO_2 interlayer isn't induced by visible light, it is used as a support and connector between Bi_2O_3 layers and g-C_3N_4 particles to improve the separation of electron–hole pairs. Key steps of the sequence of PEC reactions can be summarized as follows:

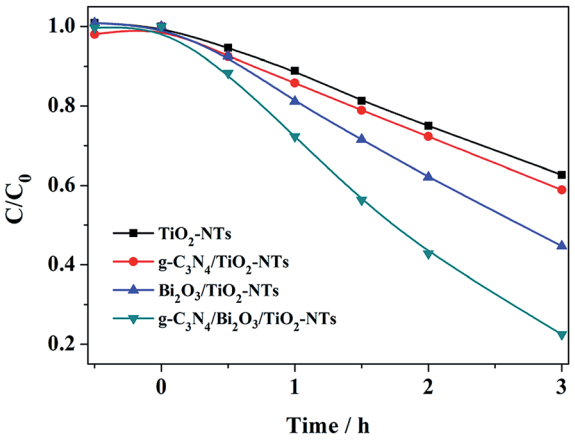

Fig. 12 The variation of [MB] *vs.* time at the TiO_2-NTs, g-C_3N_4/TiO_2-NTs, Bi_2O_3/TiO_2-NTs, g-C_3N_4/Bi_2O_3/TiO_2-NTs electrodes in PEC process with visible light irradiation. Applied potential: 3.0 V. Electrolyte: 0.1 M Na_2SO_4, pH = 7.6.

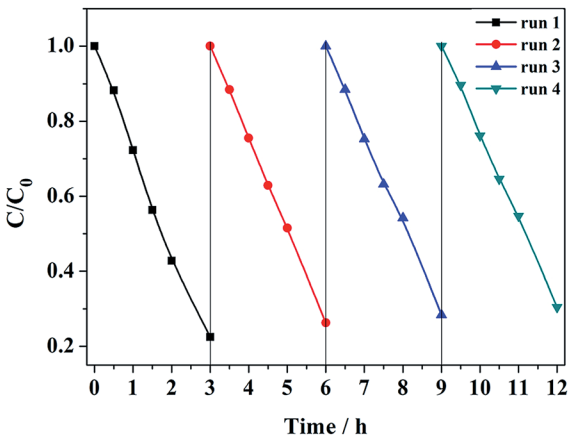

Fig. 13 Stability of the g-C_3N_4/Bi_2O_3/TiO_2-NTs electrode for PEC degradation of MB experiments with visible light irradiation at an applied potential of 3.0 V. Electrolyte: 0.1 M Na_2SO_4, pH = 7.6.

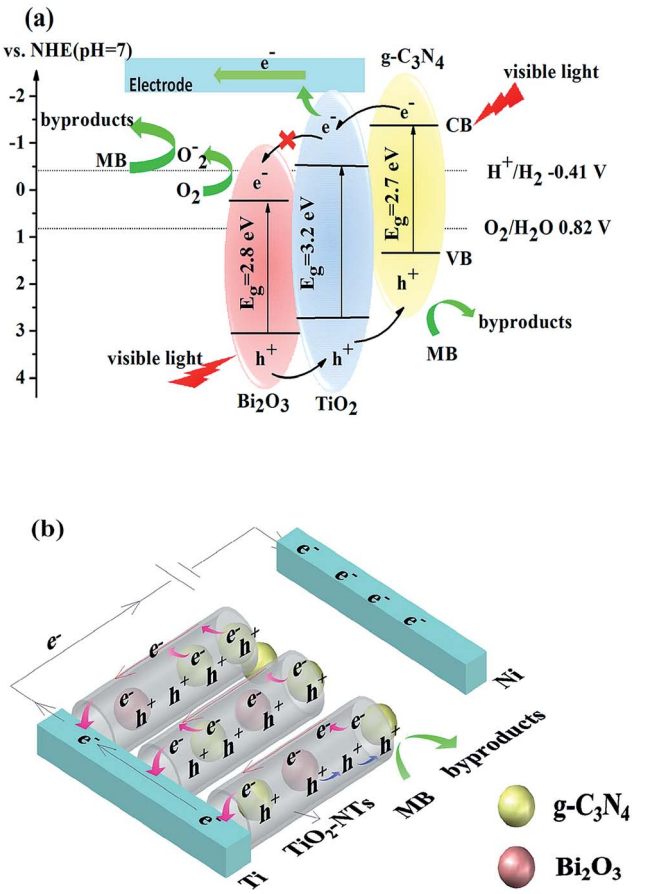

Fig. 14 One of suggested mechanism of charge separation and electron transfer in g-C_3N_4/Bi_2O_3/TiO_2-NTs electrodes under visible light irradiation.

$$Bi_2O_3 + h\nu \rightarrow Bi_2O_3\ (h^+ + e^-) \quad (3)$$

$$g\text{-}C_3N_4 + h\nu \rightarrow g\text{-}C_3N_4\ (h^+ + e^-) \quad (4)$$

$$Bi_2O_3\ (h^+) + TiO_2 \rightarrow TiO_2\ (h^+) + Bi_2O_3 \quad (5)$$

$$TiO_2\ (h^+) + g\text{-}C_3N_4 \rightarrow g\text{-}C_3N_4\ (h^+) + TiO_2 \quad (6)$$

$$g\text{-}C_3N_4\ (e^-) + TiO_2 \rightarrow TiO_2\ (e^-) + g\text{-}C_3N_4 \quad (7)$$

$$TiO_2\ (e^-) + \text{bias voltage} \rightarrow TiO_2 + \text{external circuit} \quad (8)$$

$$Bi_2O_3\ (e^-) + O_2 \rightarrow Bi_2O_3 + O_2^{\cdot -} \quad (9)$$

Of course, two of these three substances (TiO_2, Bi_2O_3 and C_3N_4) composited together, the electron–holes also could be transferred from high energy band to low energy band. So some other phenomenon, such as electrons transferred from C_3N_4 to TiO_2 or from TiO_2 to C_3N_4, was described in Fig. 14(b).

4. Conclusion

g-C_3N_4 and Bi_2O_3 with TiO_2-NTs have been coupled into a composite photocatalytic and electrocatalytic material through a sequential dip-coating procedure followed by high-temperature annealing. After adding g-C_3N_4 and Bi_2O_3, in to the host matrix, the absorption spectrum of g-C_3N_4/Bi_2O_3/TiO_2-NTs electrode red-shifted in to visible region of electromagnetic spectrum, resulting in an increase in light absorbance. Compared to naked TiO_2-NTs, photocurrent response of g-C_3N_4/Bi_2O_3/TiO_2-NTs was enhanced by 15 times and PEC activity for pollutants degradation was also improved. The enhancement in the PEC and IPCE activities was most likely due to the narrowing of the effective E_g coupled with a positive shift of E_{fb} (*ca.* 0.35 V). These results indicated that the g-C_3N_4/Bi_2O_3/TiO_2-NTs composite electrodes have the potential for wastewater treatment during PEC process under visible light irradiation.

Acknowledgements

This work was financially supported by the National Natural Science Foundation of China (no. 21276235, 21477114). In addition support was provided by the Educational Commission of Zhejiang Province (Y201432049).

References

1 M. R. Hoffmann, S. T. Martin, W. Y. Choi and D. W. Bahnemann, *Chem. Rev.*, 1995, **95**, 69–96.
2 X. B. Chen, S. H. Shen, L. J. Guo and S. S. Mao, *Chem. Rev.*, 2010, **110**, 6503–6570.
3 H. Bao, F. F. Li, L. C. Lei, B. Yang and Z. J. Li, *RSC Adv.*, 2014, **4**, 27277–27280.
4 A. J. Bard and M. A. Fox, *Chem. Res.*, 1995, **28**, 141–145.
5 B. A. Pinaud, J. D. Benck, L. C. Seitz, A. J. Forman, Z. Chen, T. G. Deutsch, B. D. James, K. N. Baum, G. N. Baum, S. Ardo, H. L. Wang, E. Miller and T. F. Jaramillo, *Energy Environ. Sci.*, 2013, **6**, 1983–2002.
6 Q. Liu, D. Wu, Y. Zhou, H. B. Su, R. Wang, C. F. Zhang, S. C. Yan, M. Xiao and Z. G. Zou, *ACS Appl. Mater. Interfaces*, 2014, **6**, 2356–2361.
7 Q. Li, B. D. Guo, J. G. Yu, J. R. Ran, B. H. Zhang, H. J. Yan and J. R. Gong, *J. Am. Chem. Soc.*, 2011, **133**, 10878–10884.
8 G. Liu, L. Z. Wang, H. G. Yang, H. M. Cheng and G. Q. Lu, *J. Mater. Chem.*, 2010, **20**, 831–843.
9 F. E. Osterloh, *Chem. Mater.*, 2008, **20**, 35–54.
10 X. B. Chen, L. Liu, P. Y. Yu and S. S. Mao, *Science*, 2011, **331**, 746–750.
11 H. Yamashita, M. Harada, J. Misaka, M. Takeuchi, K. Ikeue and M. Anpo, *J. Photochem. Photobiol. A: Chem.*, 2002, **148**, 257–261.
12 J. C. Yu, G. S. Li, X. C. Wang, X. L. Hu, C. W. Leung and Z. D. Zhang, *Chem. Commun.*, 2006, **25**, 2717–2719.
13 C. W. H. Dunnill, Z. A. Aiken, J. Pratten, M. Wilson, D. J. Morgan and I. P. Parkin, *J. Photochem. Photobiol. A: Chem.*, 2009, **207**, 244–253.
14 Y. X. Zhao, X. F. Qiu and C. Burda, *Chem. Mater.*, 2008, **20**, 2629–2636.
15 Q. Kang, S. H. Liu, L. X. Yang, Q. Y. Cai and C. A. Grimes, *ACS Appl. Mater. Interfaces*, 2001, **3**, 746–749.
16 K. Maeda and K. Domen, *J. Phys. Chem. C*, 2007, **111**, 7851–7861.
17 K. Mogyorósi, Á. Kmetykó, N. Czirbus, G. Veréb, P. Sipos and A. Dombi, *React. Kinet. Catal. Lett.*, 2009, **98**, 215–225.
18 Y. C. Yang, J. W. Wen, J. H. Wei, R. Xiong, J. Shi and C. X. Pan, *ACS Appl. Mater. Interfaces*, 2013, **5**, 6201–6207.
19 Z. H. Zhao, J. Tian, D. Z. Wang, X. L. Kang, Y. H. Sang, H. Liu, J. Y. Wang, S. W. Chen, R. I. Boughton and H. D. Jiang, *J. Mater. Chem.*, 2012, **22**, 23395–23403.
20 J. G. Hou, C. Yang, Z. Wang, S. Q. Jiao and H. M. Zhu, *Appl. Catal., B*, 2013, **129**, 333–341.
21 G. T. Yan, M. Zhang, J. Hou and J. J. Yang, *Mater. Chem. Phys.*, 2011, **129**, 553–557.
22 X. S. Zhou, B. Jin, S. S. Zhang, H. J. Wang, H. Yu and F. Peng, *Electrochem. Commun.*, 2012, **19**, 127–130.
23 X. C. Wang, K. Maeda, A. Thomas, K. Takanabe, G. Xin, J. M. Carlsson, K. Domen and M. Antonietti, *Nat. Mater.*, 2009, **8**, 76–82.
24 J. Y. Zhang, Y. H. Wang, J. Jin, J. Zhang, Z. Lin, F. Huang and J. G. Yu, *ACS Appl. Mater. Interfaces*, 2013, **5**, 10317–10324.
25 J. Wang and W. D. Zhang, *Electrochim. Acta*, 2012, **71**, 10–16.
26 X. S. Zhou, B. Jin, L. D. Li, F. Peng, H. J. Wang, H. Yu and Y. P. Fang, *J. Mater. Chem.*, 2012, **22**, 17900–17905.
27 S. Shamaila, A. K. L. Sajjad, F. Chen and J. L. Zhang, *Appl. Catal., B*, 2010, **94**, 272–280.
28 Y. Bessekhouad, D. Robert and J.-V. Weber, *Catal. Today*, 2005, **101**, 315–321.
29 Z. F. Bian, J. Zhu, S. H. Wang, Y. Cao, X. F. Qian and H. X. Li, *J. Phys. Chem. C*, 2008, **112**, 6258–6262.
30 Y. J. Cui, Z. X. Ding, P. Liu, M. Antonietti, X. Z. Fu and X. C. Wang, *Phys. Chem. Chem. Phys.*, 2012, **14**, 1455–1462.
31 J. L. Hu, H. M. Li, C. J. Huang, M. Liu and X. Q. Qiu, *Appl. Catal., B*, 2013, **142–143**, 598–603.

32 A. Ghicov, H. Tsuchiya, J. M. Macak and P. Schmuki, *Electrochem. Commun.*, 2005, **7**, 505–509.
33 Y. L. Su, S. Han, X. W. Zhang, X. Q. Chen and L. C. Lei, *Mater. Chem. Phys.*, 2008, **110**, 239–246.
34 S. S. Zhao, S. Chen, H. T. Yu and X. Quan, *Sep. Purif. Technol.*, 2012, **99**, 50–54.
35 K. H. Reddy, S. Martha and K. M. Parida, *RSC Adv.*, 2012, **2**, 9423–9436.
36 M. N. Gómez-Cerezo, M. J. Mssũnoz-Batista, D. Tudelab, M. Fernández-García and A. Kubacka, *Appl. Catal., B*, 2014, **156–157**, 307–313.
37 K. Uchida and A. Ayame, *Surf. Sci.*, 1996, **357**, 170–178.
38 A. Hameed, T. Montini, V. Gombac and P. Fornasiero, *J. Am. Chem. Soc.*, 2008, **130**, 9658–9659.
39 H. M. Zhu, B. F. Yang, J. Xu, Z. P. Fu, M. W. Wen, T. Guo, S. Q. Fu, J. Zuo and S. Y. Zhang, *Appl. Catal., B*, 2009, **90**, 463–469.
40 Y. Zhang, J. N. Lu, X. P. Wang, Q. Xin, Y. Q. Cong, Q. Wang and C. J. Li, *J. Colloid Interface Sci.*, 2013, **409**, 104–111.
41 G. P. Dai, J. G. Yu and G. Liu, *J. Phys. Chem. C*, 2011, **115**, 7339–7346.
42 M. A. Butler, *J. Appl. Phys.*, 1977, **48**, 1914–1920.
43 S. Kumar, A. G. Fedorov and J. L. Gole, *Appl. Catal., B*, 2005, **57**, 93–107.
44 Z. W. Tong, D. Yang, T. X. Xiao, Y. Tian and Z. Y Jiang, *Chem. Eng. J.*, 2015, **260**, 117–125.
45 M. N. Gómez-Cerezoa, M. J. Mũnoz-Batista, D. Tudela, M. Fernández-García and A. Kubacka, *Appl. Catal., B*, 2014, **156–157**, 307–313.
46 W. D. Zhang, L. C. Jiang and J. S. Ye, *J. Phys. Chem. C*, 2009, **113**, 16247–16253.
47 Y. Liu, Y. X. Yu and W. D. Zhang, *Electrochim. Acta*, 2012, **59**, 121–127.
48 S. D. Tilley, M. Cornuz, K. Sivula and M. Gratzel, *Angew. Chem., Int. Ed.*, 2010, **49**, 6405–6408.
49 Y. Q. Cong, M. M. Chen, T. Xu, Y. Zhang and Q. Wang, *Appl. Catal., B*, 2014, **147**, 733–740.
50 R. L. Spray, K. J. McDonald and K.-S. Choi, *J. Phys. Chem. C*, 2011, **115**, 3497–3506.
51 Y. Q. Cong, H. S. Park, H. X. Dang, F.-R. F. Fan, A. J. Bard and C. B. Mullins, *Chem. Mater.*, 2012, **24**, 579–586.
52 H. Ye, J. Lee, J. S. Jang and A. J. Bard, *J. Phys. Chem. C*, 2010, **114**, 13322–13328.
53 Y. C. Jia, P. Xiao, H. C. He, J. Y. Yao, F. L. Liu, Z. F. Wang and Y. H. Li, *Appl. Surf. Sci.*, 2012, **258**, 6627–6631.
54 X. J. Yu, L. Z. Huang, Y. C. Wei, J. Zhang, Z. Z. Zhao, W. Q. Dai and B. H. Yao, *Mater. Res. Bull.*, 2015, **64**, 410–417.
55 M. A. Rauf, M. A. Meetani, A. Khaleel and A. Ahmed, *Chem. Eng. J.*, 2010, **157**, 373–378.
56 Z. W. Tong, D. Yang, T. X. Xiao, Y. Tian and Z. Y. Jiang, *Chem. Eng. J.*, 2015, **260**, 117–125.
57 Y. F. Chen, W. X. Huang, D. L. He, Y. Situ and H. Huang, *ACS Appl. Mater. Interfaces*, 2014, **6**, 14405–14414.